Thermochimica Acta, 183 (1991) 245–268
Elsevier Science Publishers B.V., Amsterdam

Calorimetric, spectroscopic and dielectric studies of a phase transition in methylammonium hexachloroplatinate *,†

Yoshio Kume [a], Takasuke Matsuo [b] and Hiroshi Suga [b]

[a] *Faculty of General Education, Azabu University, 1-17-71, Fuchinobe, Sagamihara, Kanagawa (Japan)*
[b] *Department of Chemistry and Microcalorimetry Research Center, Faculty of Science, Osaka University, Toyonaka, Osaka (Japan)*

(Received 14 September 1990)

Abstract

The heat capacity of $(CH_3NH_3)_2[PtCl_6]$ was measured from 15 to 300 K. A phase transition was found at $T_c = 123.82 \pm 0.05$ K. An anomalous λ-type heat capacity was separated from the vibrational baseline using normal mode frequencies of the ions and lattice vibrations. The enthalpy and entropy of the transition are 1.49 kJ mol^{-1} and 14.5 J K^{-1} mol^{-1} respectively. The excess heat capacity ΔC diverged at T_c following the equation $\Delta C = A|(T - T_c)/T_c|^{-\alpha}$ where $A = 24.3 \pm 0.4$ J K^{-1} mol^{-1}, $T_c = 123.87 \pm 0.01$ K, $\alpha = 0.221 \pm 0.004$ for $T < T_c$ and $A = 3.0 \pm 0.1$ J K^{-1} mol^{-1}, $T_c = 123.77 \pm 0.02$ K, $\alpha = 0.36 \pm 0.01$ for $T > T_c$. The methylammonium ion rotates rapidly about its molecular axis, as deduced from IR line broadening, the orientational correlation time being about 1 ps at 140 K. The activation energy of the reorientation was 3.5 ± 0.1 kJ mol^{-1} as derived from three different modes of vibration of $CH_3NH_3^+$ and $CH_3ND_3^+$. The dielectric permittivity followed the excess entropy, but not the excess enthalpy, when plotted as a function of temperature in a normalized form. In contrast with Curie–Weiss behaviour, most of the change in permittivity associated with the transition occurred below T_c. This may involve a hitherto unknown mechanism of dielectric response of a molecular ionic system.

INTRODUCTION

A large number of molecular and molecular ionic crystals are known to undergo phase transitions of various types which may be regarded as resulting from the interplay between the energy and entropy of the molecular system. At low temperatures, the molecules orient themselves in such a way that their interaction energy is minimized. At higher temperatures, the

* Paper presented at the Second Japan–China Joint Symposium on Calorimetry and Thermal Analysis, 30 May–1 June 1990, Osaka, Japan.
† Contribution No. 32 from the Microcalorimetry Research Center.

0040-6031/91/$03.50

entropy term contributes to lowering the free energy of a disordered phase. A phase transition occurs at a temperature where the entropy term just outweighs the energy term. This thermodynamic description of a phase transition is simple, basically correct and applies to any thermally driven phase transitions. However, if one wants to understand the molecular mechanism of a phase transition in more detail, one finds it impossible to identify the specific molecular interaction which is responsible for the ordering of the molecules even when the crystal structure is known. This is because an apparently minor change in the molecular property causes a gross difference in the bulk property. An example of this is found in KCN and RbCN: these chemically very similar substances crystallize in the same structure (the rock salt structure) but they behave quite differently at low temperatures. There are many other similar examples of a minor chemical difference causing a remarkable change in the properties of the crystalline phase. It is therefore surprising that a group of compounds $(CH_3NH_3)_2[MX_6]$, where M = Sn, Pb, Se, Pd or Pt, and X = Cl, Br or I, form isomorphous crystals and undergo phase transitions of a similar nature at temperatures remarkably close to each other [1,2].

In previous calorimetric and structural studies of $(CH_3NH_3)_2[SnCl_6]$ and $(CD_3ND_3)_2[SnCl_6]$ [3–5], it was shown that the phase transition is basically a rotational order–disorder change of the methylammonium ion. The present paper reports the calorimetric, IR spectroscopic and dielectric studies of $(CH_3NH_3)_2[PtCl_6]$ in which the calorimetric and vibrational spectroscopic properties are examined in detail and compared with those of the analogous tin compound. The dielectric property is a new aspect of the phase transition to be studied in this series of compounds. Previous studies of the present compound include proton magnetic resonance [6], IR spectroscopy [7] and chlorine quadrupole resonance [2].

EXPERIMENTAL

Sample preparation

Chloroplatinic acid was neutralized with monomethylamine aqueous solution. The orange coloured solution was kept in a desiccator with phosphorus pentoxide. The orange crystals of $(CH_3NH_3)_2[PtCl_6]$ formed as the water evaporated. They were recrystallized in the same way.

Calorimetry

The heat capacity of $(CH_3NH_3)_2[PtCl_6]$ was measured with an adiabatic calorimeter [8] in the temperature range between 15 and 300 K. The accuracy of the measurement has been estimated to be $\pm 0.2\%$ or better

between 80 and 300 K and approximately ±1% at 20 K. The mass of the sample was 8.231 g. The temperature steps of the measurement were 1–3 K except in the vicinity of the transition point where they were reduced to 0.1 K or less in order to avoid distortion of the heat capacity peak by averaging over too large a temperature interval.

IR spectra

IR spectra were recorded at temperatures between 80 and 300 K in the 400–4000 cm^{-1} frequency range. It was found that the linewidth of the internal vibration of $CH_3NH_3^+$ belonging to the E species depends strongly on temperature. Therefore, they were examined closely as a function of temperature. A thermocouple junction was embedded in a hole drilled in one of the KBr discs between which the polycrystalline sample mulled in Nujol was sandwiched. The sample was maintained within ±0.7 K of the intended temperature. Spectra of $(CH_3ND_3)_2[PtCl_6]$ were also studied because some of the normal modes were stronger and at more convenient frequencies in the deuterated than in the normal compound.

Dielectric permittivity

The sample was pressed into a disc 12 mm in diameter and 0.80 mm thick and annealed at 100 °C in vacuo for 24 h. Circular pieces of gold foil (6.0 mm in diameter) were attached to the faces with a small amount of Apiezon grease. A guard electrode was not used. The fringe effect was corrected for in the calculation of the permittivity from the capacitance. The sample was placed in a doubly thermostatted cryostat whose temperature stability was within ±0.05 K of the set point. The accuracy of the temperature scale measured with a chromel–constantan thermocouple was about ±0.1 K at 300–80 K and probably not worse than ±0.3 K at 20.4 K, the lowest temperature of the dielectric measurement. The capacitance of the sample was measured with a bridge (General Radio Model 1620A) at frequencies between 100 Hz and 100 kHz. However, the dielectric permittivity turned out to be independent of the frequency, and therefore the bulk of the measurements were made at 1 kHz.

EXPERIMENTAL RESULTS

Heat capacity

Figure 1 shows the heat capacity of $(CH_3NH_3)[PtCl_6]$, and the numerical values are given in Table 1. The λ transition started to contribute to the heat

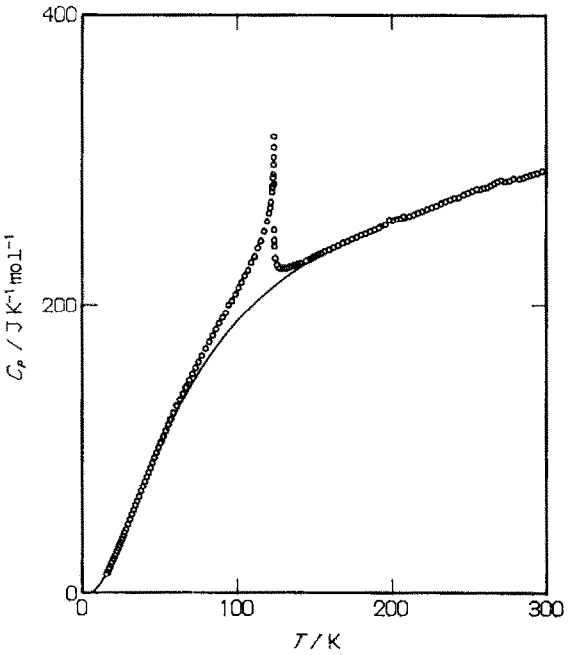

Fig. 1. Heat capacity of methylammonium hexachloroplatinate.

capacity at about 60 K and reached its peak at $T_c = 123.8$ K. At $T > T_c$, there is also a small but significant effect of the phase transition (the short-range order effect). Slight irregularities near 200 and 270 K are due to melting of the occluded aqueous solution. These irregularities were initially larger than are shown in Fig. 1. After the first measurement was completed, the sample was taken out, ground and dried by heating under reduced pressure. The heat capacity determined thereafter showed reduced irregularities. The data near the λ peak reported here are those obtained in the first measurement, because mechanical disturbance imparted to the crystal by grinding is known to cause severe broadening of the peak of the heat capacity [4]. Figure 2 shows the heat capacity for the 4 K interval covering the peak. Two points are to be noted. First, as the peak temperature was approached, the heat capacity increased with an increasing slope. This indicates that any broadening effects are insignificant outside the temperature step (about 0.1 K) of the measurement, even though the measurement was performed on an as-grown crystal aggregate. The second point to be noted is the behaviour above T_c. Even though the heat capacity decreased rapidly above T_c, it was not a discontinuous decrease. The phase transition is thus a critical point (or close to one) rather than a phase transition of the second order, as defined by Ehrenfest. No latent heat of the phase transition was found either. The curves drawn in Fig. 2 are the best-fit theoretical expression of the divergent heat capacity discussed below.

TABLE 1

Experimental heat capacities of methylammonium hexachloroplatinate

T (K)	C_p ($J\,K^{-1}\,mol^{-1}$)	T (K)	C_p ($J\,K^{-1}\,mol^{-1}$)	T (K)	C_p ($J\,K^{-1}\,mol^{-1}$)
Series 1		119.37	257.4	240.12	273.3
15.25	13.94	120.49	263.1	242.90	273.7
15.51	14.53	121.21	266.8	246.01	275.6
16.07	15.34	121.73	270.7	248.98	276.9
16.88	17.49	122.48	277.3	251.74	278.2
17.71	19.17	122.72	280.5	254.62	279.5
18.57	21.51	122.82	281.9	256.77	279.2
19.35	23.21	123.11	287.2	259.01	280.0
20.06	24.77	123.21	289.5	261.25	280.6
20.87	26.88	123.42	296.3	263.47	281.9
21.76	29.07	123.51	301.4	265.70	283.3
22.58	30.98	123.61	308.3	268.00	284.5
23.35	32.94	123.70	315.6	270.37	285.6
23.89	34.59	123.78	282.9	272.93	284.8
24.50	36.07	123.87	251.5	275.70	285.2
25.35	38.23	123.96	244.4	278.46	286.8
26.14	40.20	124.05	240.2	282.17	286.4
26.98	42.60	124.56	232.3	284.39	287.1
27.98	45.02	125.72	227.7	286.61	288.2
29.18	48.55	126.84	225.9	288.82	289.1
30.50	51.93	127.40	225.4	291.03	289.8
31.77	55.46	128.58	225.1	293.38	290.5
32.95	58.48	130.41	225.3	297.07	291.9
34.05	61.65	132.23	225.4	300.36	292.8
35.08	64.39	134.04	226.1		
36.31	67.67	135.92	226.9	Series 2	
37.71	71.44	137.31	227.2	120.16	261.2
39.02	75.00	137.70	227.1	120.33	261.8
40.28	78.33	137.87	227.5	120.49	263.1
41.51	81.51	138.08	227.1	120.64	263.6
42.67	84.57	138.84	227.7	120.83	264.7
43.85	87.78	139.35	228.1	121.04	265.9
45.13	91.08	141.15	229.1	121.21	266.8
46.48	94.62	144.66	230.4	121.31	267.9
47.85	98.21	145.91	230.8	121.42	268.0
49.10	101.7	147.15	231.5	121.52	268.9
50.31	104.7	148.40	232.4	121.62	269.6
50.96	105.9	149.64	233.1	121.73	270.7
52.35	109.4	150.87	233.7	121.83	271.0
53.84	113.1	152.51	234.6	121.94	272.5
55.44	117.1	154.38	235.5	122.04	272.9
56.97	120.6	156.69	236.9	122.14	273.8
58.79	125.0	159.45	238.0	122.17	273.9
60.89	129.8	162.30	239.6	122.33	275.9
62.90	134.4	165.35	240.9	122.48	277.3
64.83	138.6	168.35	242.6	122.61	278.8

TABLE 1 (continued)

T (K)	C_p ($J\,K^{-1}\,mol^{-1}$)	T (K)	C_p ($J\,K^{-1}\,mol^{-1}$)	T (K)	C_p ($J\,K^{-1}\,mol^{-1}$)
66.69	142.7	171.33	243.7	122.72	280.5
67.22	144.0	174.28	245.3	122.82	281.9
68.98	147.7	177.23	246.4	122.91	282.8
71.02	152.1	180.15	248.0	123.01	285.0
73.00	156.2	183.06	249.1	123.11	287.2
74.92	160.3	185.95	250.5	123.21	289.5
77.08	164.7	188.82	251.6	123.31	292.5
79.46	169.5	191.69	252.9	123.42	296.3
81.77	174.2	192.85	254.0	123.51	301.4
84.01	178.6	195.72	255.3	123.61	308.3
86.20	183.0	198.28	258.6	123.70	315.6
88.33	187.1	200.48	258.2	123.78	282.9
90.42	191.0	202.73	259.0	123.87	251.5
92.46	194.2	204.98	259.5	123.96	244.4
94.46	200.0	207.22	260.9	124.05	240.2
96.55	203.0	208.33	260.3	124.14	237.8
98.74	207.4	211.10	261.1	124.23	236.1
100.86	212.0	213.87	262.2	124.33	234.4
102.91	215.7	216.63	263.5	124.42	233.8
104.93	220.2	219.50	264.4	124.56	232.3
107.02	223.9	222.51	265.9	124.78	230.9
109.16	229.3	225.50	267.0	125.00	229.9
111.27	233.3	228.48	268.1	125.22	229.0
113.35	239.3	231.45	269.7	125.45	228.2
115.39	243.9	234.41	270.9	125.72	227.7
117.39	250.4	237.35	272.3		

IR spectra

The spectral region studied contains the internal vibrations of the methylammonium ion. The frequencies agreed well with those reported by Oxton and Knop [7]. They are used in the analysis of the heat capacity discussed below. Figure 3 shows the absorption band shapes of ν_{12} of $CH_3ND_3^+$ recorded at several temperatures. They are obviously temperature dependent. It was found that the line shape of the totally symmetric modes for which the transition dipole vector points parallel to the C_{3v} axis is not particularly temperature dependent. A theory describing the symmetry-dependent broadening has been formulated from group theory [9]. It was found to apply well to the present case.

Dielectric permittivity

As shown in Fig. 4, the dielectric permittivity increased gradually with increasing temperature. The slope increased as the transition temperature

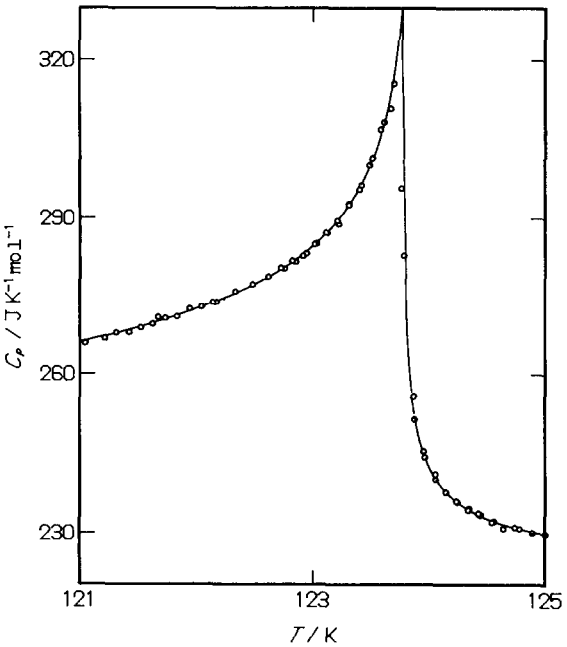

Fig. 2. Heat capacity of methylammonium hexachloroplatinate near the phase transition. The curves are the best-fit equations of the form $\Delta C = A\,|(T - T_c)/T_c\,|^{-a}$.

was approached. Above T_c, the permittivity increased linearly until $T \approx 245$ K. At higher temperatures, it increased more rapidly again (an unavoidable effect of adsorbed water). The different marks used to plot the data in Fig. 4 show the different series of measurement. Their agreement indicates the satisfactory reproducibility of the data, in particular the stability of the gold foil electrodes. The curve in Fig. 4 was calculated using the Debye internal energy function with the characteristic temperature of 66.2 K, as will be discussed below.

DISCUSSION

Calculation of the excess heat capacity and the entropy of transition

We assume that the experimental heat capacity consists of the normal and excess parts due, respectively, to the vibrational motion of the ions and to the phase transition. The normal heat capacity has to be calculated with the minimum possible arbitrariness. This was achieved by incorporating the vibrational and NMR spectroscopic data.

There are 69 vibrational degrees of freedom per unit cell containing one molecular unit of $(CH_3NH_3)_2[PtCl_6]$ [7,10]: 36 internal vibrations of the two $CH_3NH_3^+$ (abbreviated as MA^+) ions, 15 internal vibrations of the

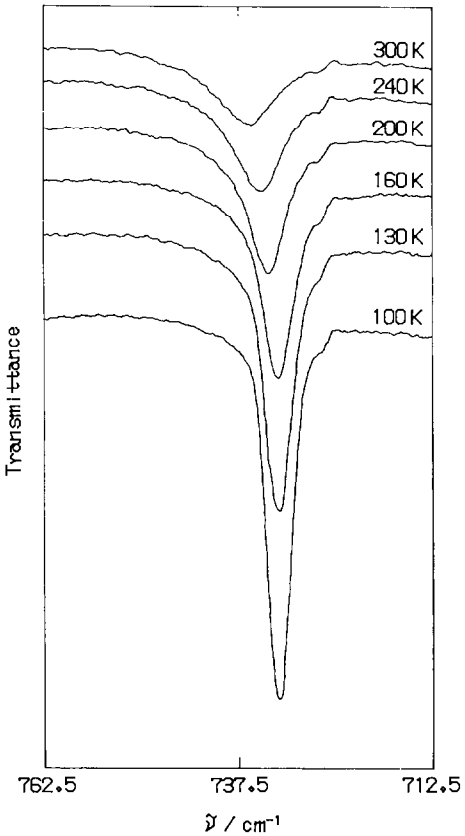

Fig. 3. IR spectra of a rocking mode of the methylammonium ion in $(CH_3ND_3)_2[PtCl_6]$.

$[PtCl_6]^{2-}$ ions and 18 lattice modes. The lattice vibrations are classified as three acoustic branches and 15 optical branches. The vibrational heat capacities were calculated by the Debye (the acoustic branches) and Einstein (the optical branches and internal modes) approximations. Some of the characteristic frequencies were taken from the spectroscopic data of $(MA)_2[PtCl_6]$. These are the internal modes of the MA^+ ion [7,11] (except the torsional vibration of A_2 symmetry (the internal rotation)) and the ν_3 and ν_4 (in the Herzberg notation) of $[PtCl_6]^{2-}$. The ν_1, ν_2, ν_5 and ν_6 frequencies of $[PtCl_6]^{2-}$ were assumed to be the same as the corresponding ones in $(NH_4)_2[PtCl_6]$ [12]. The torsional vibration of MA^+ is inactive both in IR and Raman, and has not been assigned. There is also a complication due to the coupling of the internal rotation and the rotation of the cation as a whole about the same axis. Since the barriers to the rotations are low [6], the coupled motions had to be treated fully quantum-mechanically, taking into account the symmetry of each state (see Appendix A).

There remain 16 external modes to be determined. The frequency of the rotational vibration of $[PtCl_6]^{2-}$ was assumed to be the same as in the

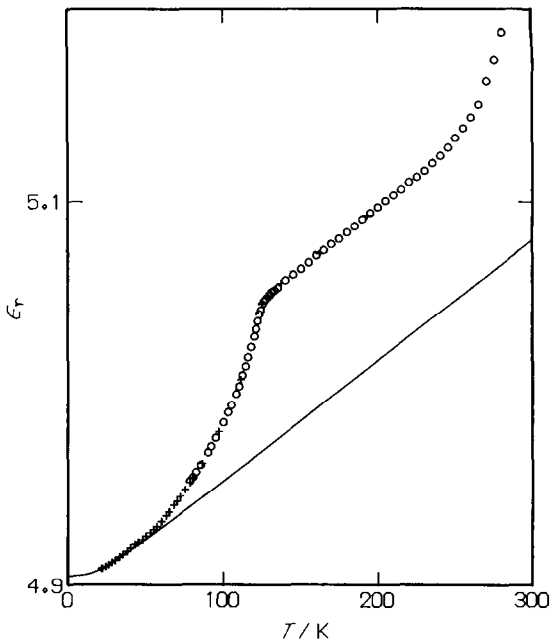

Fig. 4. Relative dielectric permittivity of methylammonium hexachloroplatinate: o, first series; ×, second series. The solid curve is the calculated one using the Debye approximation with $\theta_D = 66.2$ K.

closely related substance $(NH_4)_2[PtCl_6]$ [12]. The other 13 vibrational modes could not be deduced from spectroscopic data. They were represented with a Debye model of weight 3 and three Einstein oscillators of weights 4, 3 and 3 each. The characteristic frequencies were determined by fitting the calculated heat capacities to the experimental values outside the phase transition region. Correction for the difference between C_p and C_v was also included in the fitting. The fitting function is summarized as follows:

$$\sum_{\text{data}} \left[C_p(\text{exp}) - C_p(\text{calc})\right]^2 = \text{min.} \tag{1}$$

where

$$C_p(\text{exp}) = \text{the experimental heat capacity} \tag{2}$$

$$C_p(\text{calc}) = C_{\text{known}} + C_{\text{unknown}} + AC_p^2T \tag{3}$$

$$C_{\text{known}} = C(\text{internal vib., 49E}) + C(\text{hindered rot., 4QM}) + C\left([PtCl_6]^{2-}\ \text{rot., 3E}\right) \tag{4}$$

$$C_{\text{unknown}} = C(\text{lib., 4E}) + C(\text{trans., 6E}) + C(\text{trans., 3D}) \tag{5}$$

$$AC_p^2T = (C_p - C_v)\ \text{correction} \tag{6}$$

Here "known" means "to be calculated from the spectroscopic data", and

"unknown" means "to be determined by fitting to the heat capacity data". The numbers in parentheses represent the degrees of freedom included in the respective terms and add up to 69, as they should. The capital letters E, QM and D indicate the Einstein approximation, quantum mechanical calculation and the Debye approximation respectively. The other descriptive terms are self-explanatory.

The best-fit parameters were determined by the non-linear least-squares method [13]. The result depended on the temperature intervals of the data taken into the fitting. When the data close to the transition temperature were used, the heat capacity difference deviated systematically upward in the corresponding temperature region. The fitting was then repeated after

TABLE 2

Spectroscopic data used in the calculation of the vibrational heat capacity

Frequency (cm^{-1})	Weight		
MA^+ internal modes [a]			
3225.6	4	N–H antisym. str.	
3188.0	2	N–H sym. str.	
2974.8	4	C–H antisym. str.	
2896.0	2	C–H sym. str.	
1581.0	4	NH_3 antisym. def.	
1469.9	2	NH_3 sym. def.	
1452.3	4	CH_3 antisym. def.	
1415.0	2	CH_3 sym. def.	
1248.9	4	Rock.	
990.0	2	C–N str.	
903.4	4	Rock.	
For torsion, see Appendix A			
$[PtCl_6]^{2-}$ internal modes			
344	1	Pt–Cl str. [b]	
331	3	Pt–Cl str. + def. [c]	
315	2	Pt–Cl str. [b]	
189	3	Pt–Cl str. [c]	
180	3	Def. [b]	
82	3	Def. [b]	
Lattice modes			
69	3	$[PtCl_6]^{2-}$ rot. [b]	
185.2	3	Translational optical	fitted
135.7	4	MA^+ lib.	fitted
106.7	3	Translational optical	fitted
$\theta_D = 66.2$ K	3	Translational acoustic	fitted
$C_p - C_v = AC_pT^2$	$A = 5.80 \times 10^{-8}$ mol J^{-1}		fitted
For C_3 rot. of MA^+, see Appendix A			

[a] Ref. 7.

[b] Ref. 12.

[c] Determined with a Nicolet Model 170FX spectrometer at Nicolet Japan Inc.

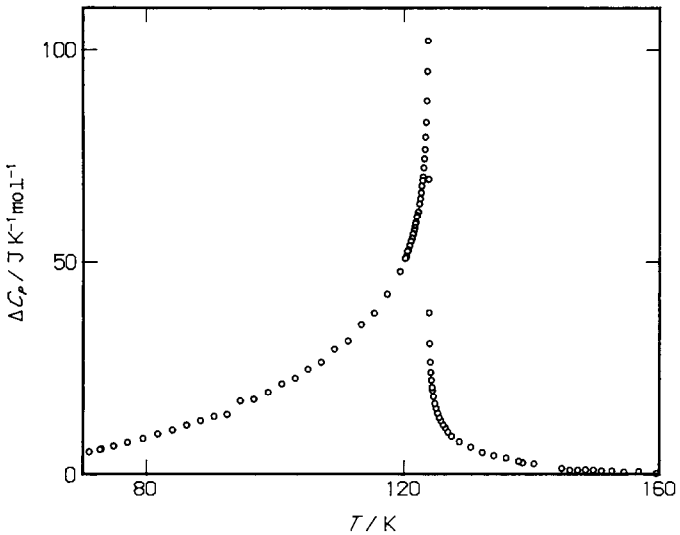

Fig. 5. Excess heat capacity of methylammonium hexachloroplatinate due to the phase transition.

the influenced data were removed. In the final refinement where there were no more systematic deviations, 96 data points distributed between 15 and 42 K and between 171 and 300 K were used. The parameter values thus determined are listed in Table 2 together with the spectroscopic data used in the fitting. The $\nu_E(4)$ Einstein frequency, 135.7 cm^{-1}, may be identified with the frequency of the librational motion in which the C–N axis of the cation oscillates about the C_3 axis of the crystal. The two Einstein frequencies may similarly be interpreted as the frequencies of the translational optical mode averaged over the Brillouin zone.

The solid curve in Fig. 1 represents the normal heat capacity thus calculated. The excess heat capacity determined by subtraction of the normal from the experimental heat capacity is plotted in Fig. 5. Integration of the curve gave the transition enthalpy, transition entropy and the critical entropy ratio as follows:

$T_{trs} = 123.82 \pm 0.05$ K

$\Delta_{trs}H = 1.49$ kJ mol^{-1}

$\Delta_{trs}S = 14.5$ J K^{-1} mol^{-1}

Hence

$$\frac{\Delta_{trs}S - \Delta_{trs}S(T_{trs})}{\Delta_{trs}S} = 0.0921$$

Mechanism of the transition

The transition entropy, 14.5 J K^{-1} mol^{-1}, is equal to R ln 5.72. This indicates that the transition is of an order–disorder type. If the present crystal is isostructural with $(CD_3ND_3)_2[SnCl_6]$, which is very likely, the MA^+ ion is disordered over a pair of symmetry-related positions, one of which is reached from the other by rotation about the C–N axis. It is most probable that the phase transition is caused by the ordering of the disordered MA^+ ion into a uniquely determined position. The transition entropy will be equal to $2R$ ln $2 = 11.52$ J K^{-1} mol^{-1}. The experimental value, 14.5 J K^{-1} mol^{-1}, is about 25% larger than this, but it supports the basic order–disorder mechanism. The mechanism is also consistent with the IR and dielectric properties discussed below.

Critical properties

The anomalous heat capacity increased on both sides of the transition temperature as shown in Fig. 2. This behaviour is described by the equation [14]

$$\Delta C = A\,|(T - T_c)/T_c\,|^{-\alpha} \tag{7}$$

where A, T_c and α are, according to our present knowledge, parameters to be determined experimentally. For $T < T_c$ (121.5 K $\leqslant T < T_c$) the best-fit values are $A = 24.3 \pm 0.4$ J K^{-1} mol^{-1}, $T_c = 123.87 \pm 0.01$ K and $\alpha = 0.221 \pm 0.004$; for $T > T_c$ ($T_c < T \leqslant 124.8$ K) the best-fit values are $A = 3.0 \pm 0.1$ J K^{-1} mol^{-1}, $T_c = 123.77 \pm 0.02$ K and $\alpha = 0.36 \pm 0.01$. These were determined by the least-squares fit of eqn. (7) in the logarithmic form using the data points between 121.5 and 123.6 K for $T < T_c$ and those between 123.8 and 124.8 K for $T > T_c$. The logarithmic plots are linear as shown in Fig. 6. The calculated heat capacities are also shown in Fig. 2 plotted as solid curves. We had to choose different values of T_c for $T > T_c$ and $T < T_c$. The difference between them is approximately equal to the temperature step of the C_p measurements: this is not apparent in Fig. 2. Table 3 gives numerical values related to the critical properties of the phase transitions in the chloroplatinate and chlorostannates. One sees that the critical properties are very similar among these substances. A theoretical interpretation of these values has not been carried out yet. From the experimental point of view, there are two other types of critical behaviour in molecular and molecular ionic crystals. In one, the heat capacity increases gradually at low temperatures and then jumps abruptly to infinity (or becomes undefined) as the substance undergoes a first-order phase transition. For most phase transitions of this type, the excess heat capacity above T_c is small or practically absent. Typical examples are NH_4Cl [15], KH_2PO_4 [16], TlH_2PO_4 [17] and $(thiourea)_3CCl_4$ [18]. In these substances, the short-range fluctuation effect

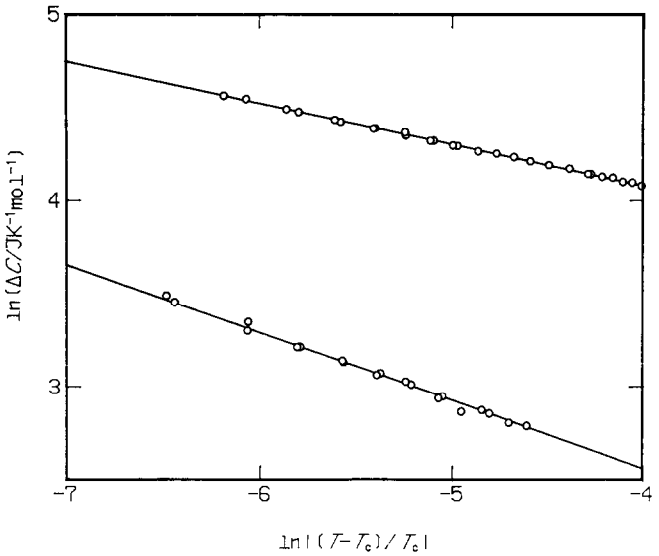

Fig. 6. Logarithmic plot of the excess heat capacities of methylammonium hexachloroplatinate. Upper line $T < T_c$, lower line $T > T_c$.

(the excess C_p above T_c) may be swamped by the first-order transition. An exceptional case occurs in $SnCl_2 \cdot 2H_2O$ in which the excess heat capacity is symmetrical about T_c but the phase transition is first-order, characterized by a discontinuity in the entropy and enthalpy [19,20]. Another type of behaviour is that in which the heat capacity increases gradually below T_c and decreases abruptly at T_c, undergoing a discontinuity. We found phase transitions of this type in $K_4Fe(CN)_6 \cdot 3H_2O$ [21–23], $(trisarcosine)_3CaCl_2$ [24], $NH_4H(COO)_2 \cdot 1/2H_2O$ [25], $ND_4H(COO)_2 \cdot 1/2D_2O$ [25], CH_3NH_3I [26] and anilinium halide [27]. The Landau theory of phase transitions of the second kind predicts this type of behaviour.

The present substance lies between these two groups with respect to the critical properties, with the heat capacity increasing to very large values, apparently limited only by the resolution of the calorimetry. It should be added that a detailed analysis of divergent heat capacities has been reported recently on compounds containing the MA^+ ion [28,29].

IR absorption line shape

The double-beam spectrometer recorded the relative transmitted intensity I/I_0, where I and I_0 are the transmitted and incident IR intensities. The absorbance $a(\nu)$ is related to I_0/I by taking its logarithm:

$$a(\nu) = a_0 \ln(I_0/I) \tag{8}$$

Since we are not interested in the absolute absorbance, a_0 is merely a proportionality constant.

TABLE 3

Critical properties of $(CH_3NH_3)_2[PtCl_6]$ and related compounds

	$T > T_c$			$T < T_c$			$[S(\infty) - S(T_c)]/S(\infty)$	Ref.
	T_c (K)	A (J K^{-1} mol^{-1})	α	T_c (K)	A (J K^{-1} mol^{-1})	α		
$(CH_3NH_3)_2[PtCl_6]$	123.765	3.03	0.36	123.868	24.3	0.221	0.092	This work
$(CH_3NH_3)_2[SnCl_6]$	154.32		0.36	154.32		0.19	0.063	3
$(CD_3ND_3)_2[SnCl_6]$	154.925	0.966	0.65	155.27	31.08	0.24	0.110	4
$(CH_3NH_3)_2NaSO_4 \cdot 6H_2O$	139.35		0.36					28

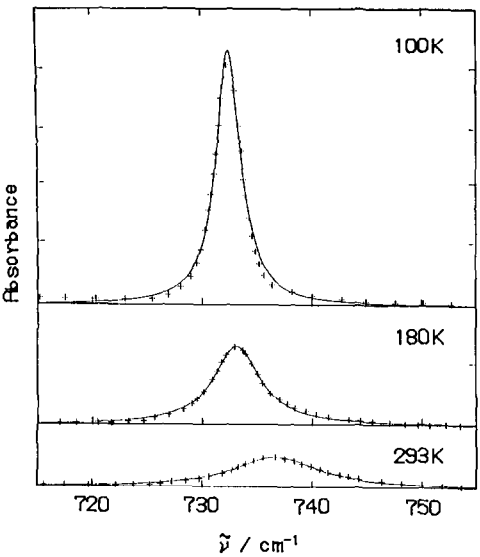

Fig. 7. IR absorbance of the rocking vibration of the methylammonium ion in $(CH_3ND_3)_2[PtCl_6]$ at three temperatures.

As described in the experimental section, the linewidth of the E modes of MA^+ ion was temperature dependent. This indicates that the width has a motional origin in the anisotropic rotation of the cation. We fitted the Lorentzian line shape function to the absorbance of the rocking (about 910 cm^{-1}) of MA^+, and the methyl rocking (1188 cm^{-1}) and ammonium rocking (about 730 cm^{-1}) of $CH_3ND_3^+$ in $(MA)_2[PtCl_6]$. For the fitting, the following quantity was minimized:

$$F(A, B, C, \nu_0, \Delta\nu) = \sum \left[\ln\left(\frac{I_0}{I}\right)_{obs} - \frac{A}{(\nu - \nu_0)^2 + (\Delta\nu)^2} + B + C\nu \right]^2 \qquad (9)$$

where the first term in the square brackets is the logarithm of the inverse experimental transmittance at ν, and the second term is the Loretnzian function in which ν_0 is the frequency of the band centre and $\Delta\nu$ is the half-width at half-maximum intensity. The third and fourth terms describe background absorption which is assumed to be linear in ν. Three typical results of the fitting are shown in Fig. 7, where the absorbance of one of the rocking modes of MA^+ is plotted against frequency. The Lorentzian reproduced the experimental line shape satisfactorily.

For an E-type mode of a C_{3v} molecule, the transition dipole moment is oriented perpendicular to the symmetry axis. Therefore, if the molecule reorients frequently about the triad axis, the dipole autocorrelation function decays rapidly as a function of time. Since the Fourier transform of the autocorrelation function is proportional to the line shape function, fast reorientation (short correlation time) results in a broad absorption band.

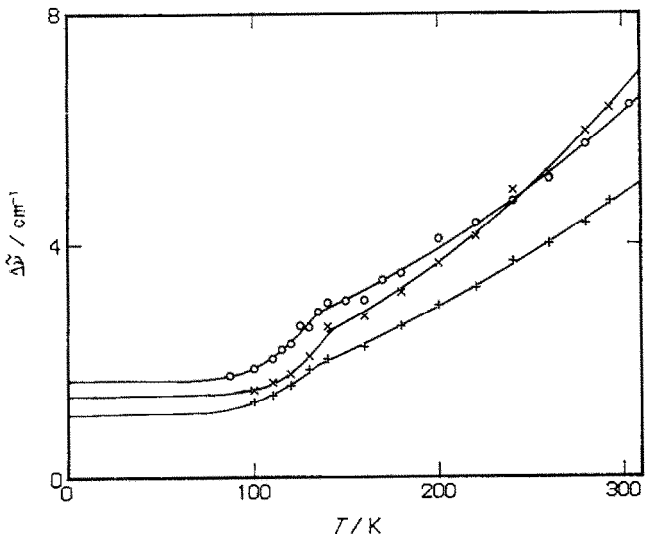

Fig. 8. Linewidth of the IR absorption spectra of the methylammonium ion (rocking modes) in $(CH_3NH_3)[PtCl_6]$ and its deuterated analogue. ○, $CH_3NH_3^+$; ×, CH_3 in $CH_3ND_3^+$; +, ND_3^+ in $CH_3ND_3^+$.

The Lorentzian derives from an exponential correlation function. The correlation time τ is related to the band width $\Delta\nu$ by

$$\tau = 1/(2\pi c\,\Delta\nu) \tag{10}$$

where c is the velocity of light in vacuo. The numerical factor $(1/2\pi)$ depends on the model of reorientation. Here rotational diffusion is assumed. Figure 8 shows $\Delta\nu$ of the rocking modes of the three isotopic molecules of MA^+ plotted against temperature. The width increased with temperature in similar ways for the three modes, though the $-ND_3$ rocking had a somewhat smaller linewidth than the other two. At low temperatures, the linewidth levelled off to approach a constant value. The residual width may represent a resultant effect of static broadening of an unknown origin and instrumental resolution.

The residual width was subtracted from the observed width to obtain the temperature-dependent width of dynamic origin. The width thus corrected for the residual width was substituted in eqn. (10) to calculate the correlation time. The correlation times thus determined are plotted in Fig. 9 in an Arrhenius plot. For $T > T_c$, the plot gave the activation energy E_a and the pre-exponential factor τ_0 as follows: $-ND_3$ rocking of $CH_3ND_3^+$, $E_a = 3.4$ kJ mol^{-1} and $\tau_0 = 0.59$ ps; $-CH_3$ rocking of $CH_3ND_3^+$, $E_a = 3.6$ kJ mol^{-1} and $\tau_0 = 0.40$ ps; and $CH_3NH_3^+$ rocking, $E_a = 3.5$ kJ mol^{-1} and $\tau_0 = 0.40$ ps.

The straight line in Fig. 9 represents the correlation time derived from the spin–lattice relaxation time of proton magnetic resonance. The activation energy and pre-exponential factor from the nuclear resonance [6] are 3.6–3.8

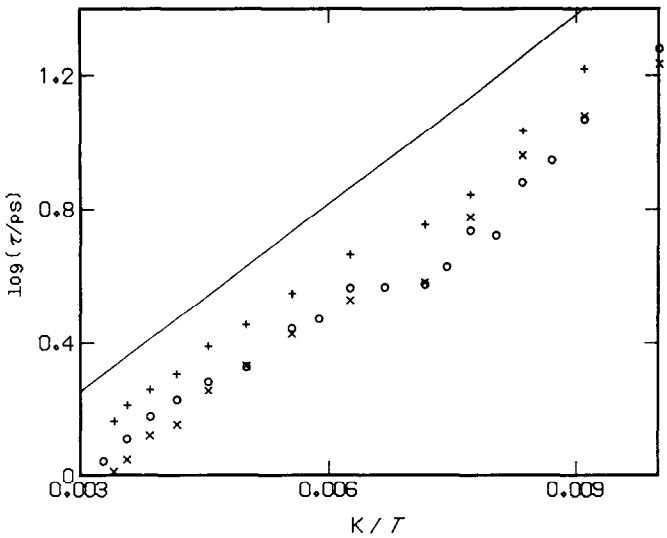

Fig. 9. Arrhenius plot of the correlation time of reorientation of the methylammonium ion in $(CH_3NH_3)_2[PtCl_6]$. ○, $CH_3NH_3^+$; ×, CH_3 in $CH_3ND_3^+$; +, ND_3^+ in $CH_3ND_3^+$.

kJ mol^{-1} and 4.5×10^{-13} s, which are in good agreement with the present values. In the proton resonance experiment, correlation times of the internal rotation have also been determined. Comparing the Arrhenius parameters, we conclude that the IR absorption linewidth is determined by the rotation of the MA^+ ion as a whole.

The linewidth near T_c was larger than that predicted by the Arrhenius plot. The opposite effect is expected because the correlation time usually increases near T_c (critical slowing-down). At present we cannot explain the non-Arrhenius temperature dependence which the three modes exhibit.

Dielectric permittivity

The dielectric permittivity of a crystal containing polar ions may be expected to follow a Curie–Weiss type temperature dependence. This is not the case for the present substance as Fig. 4 shows. The permittivity is linear in T over a considerable temperature interval above T_c. If the conductivity due to water impurity did not intervene for $T > 250$ K, the linear temperature dependence would persist over the entire high temperature region. This indicates that the phase transition does not involve ordering of the polar axis of MA^+ ions. The disorder found in $(CD_3ND_3)_2[SnCl_6]$ is of this type, involving rotation of the ion about the threefold axis and thus does not contribute to the electric polarization. The same type of disorder is most probably involved in the present substance.

The dielectric permittivity plotted in Fig. 4 was calculated from the measured capacitance using the sizes of the sample and electrodes de-

termined at 25°C. Since the sample contracts at low temperatures, the permittivity should be slightly different from those plotted in Fig. 4. The magnitude of the correction depends on whether or not the electrodes contract with the sample. We estimate the correction by assuming that they do contract with the sample, because the gold foil electrodes were very thin and probably accommodate themselves to the change in the sample size. The *a*-axis thermal expansion coefficient of $(CH_3NH_3)_2[SnCl_6]$ is 7×10^{-5} K^{-1} in the high temperature phase [30]. In the absence of expansivity data for the platinum compound, we may use the data for estimation purposes. The permittivity ϵ_r is related to the capacitance C by the equation $\epsilon_r = (L/A)(1/\epsilon_0)C$ where L is the thickness of the sample, A the area of the electrode and ϵ_0 the permittivity of the vacuum. The temperature dependence of the geometric factor $(A/L)\,\mathrm{d}(L/A)/\mathrm{d}T$ is equal to 1/3 of the volume thermal expansivity because the sample was an isotropic disc. The volume expansivity of the tin compound is 6.6×10^{-5} K^{-1} [30], while the temperature coefficient of the apparent dielectric permittivity is 12.9×10^{-5} K^{-1} between 140 and 240 K. Therefore, approximately 51% of the temperature coefficient can be explained by the geometric effect.

The thermal coefficient of the dielectric permittivity has been discussed in terms of the anharmonic lattice vibration [31]. Szigeti showed that a positive slope of $2\text{–}3 \times 10^{-4}$ K^{-1} of the static dielectric permittivity of ionic crystals (NaCl, KCl) can be explained by a Debye model of lattice vibration modified to include anharmonicity of the vibration. If the same theory applies to the present substance, the linear portion of the plot in Fig. 4 contains two anharmonicity effects, one through the thermal expansion of the sample and the other a direct anharmonicity effect.

The decrease in the permittivity below T_c cannot be explained by thermal contraction of the sample. The lattice parameters of $(CH_3NH_3)_2[SnCl_6]$ are less temperature dependent below T_c than above [30]. If we assume that the platinum compound also behaves in the same way as the tin compound in this respect, the size effect would predict a smaller temperature dependence of the apparent dielectric permittivity below T_c than above. This is the opposite of the experimental result. Therefore, we have to invoke an effect other than thermal contraction to explain the rapid decrease in the permittivity below T_c.

In order to extract the effect due to the phase transition from the experimental data, we assumed that the dielectric permittivity $\epsilon_r(T)$ is separated into vibrational and configurational parts

$$\epsilon_r(T) = \epsilon_{vib}(T) + \epsilon_{conf}(T) \tag{11}$$

where $\epsilon_{vib}(T)$ is responsible for the linear increase of the permittivity above T_c. However, this cannot be extrapolated linearly to 0 K, because it would contradict the third law of thermodynamics. We must have $\mathrm{d}\epsilon_r/\mathrm{d}T = 0$ at 0 K. A better extrapolation function is found as follows. According to the

thermodynamics of solids, the internal energy of a crystal is approximately proportional to its volume as a function of temperature. It is also a good approximation to assume that the intrinsic contribution of the anharmonicity to the permittivity is proportional to the vibrational internal energy. Therefore, we write $\epsilon_{vib}(T)$ as follows:

$$\epsilon_{vib}(T) = A + BD_E(\theta_D/T) \tag{12}$$

where A is the dielectric permittivity at 0 K, B is a proportionality constant, and $D_E(\theta_D/T)$ is the Debye internal energy function with the characteristic temperature θ_D (A and B should not be confused with those in eqn. (9)). The last quantity was determined as $\theta_D = 66.2$ K (Table 2) from the calorimetric experiment. A and B were determined so as to reproduce the slope of the permittivity in the linear region (140–240 K) where $\epsilon_{conf}(T)$ no longer changes, and also the low temperature value at 20 K where ϵ_{conf} is effectively zero. Thus

$$\epsilon_{vib}(T) = 4.906 + 6.34 \times 10^{-4} D_E(66.2\ \text{K}/T) \tag{13}$$

where the Debye energy function is normalized as follows:

$$dD_E/dT = T \quad \text{for } T \gg \theta_D \tag{14}$$

The curve plotted in Fig. 4 was calculated in this way.

The difference between ϵ_{exp} and $\epsilon_{vib}(\epsilon_{conf} = \epsilon_{exp} - \epsilon_{vib})$ is plotted in Fig. 10 in a normalized form: $\epsilon_{conf}(T)/\epsilon_{conf}(\infty)$ vs. temperature, where $\epsilon_{conf}(\infty) = 0.0797$. We have thus derived the dielectric response of the sample contributed by the molecular motion which is responsible for the phase transition. Even though the mechanism by which the type of disorder

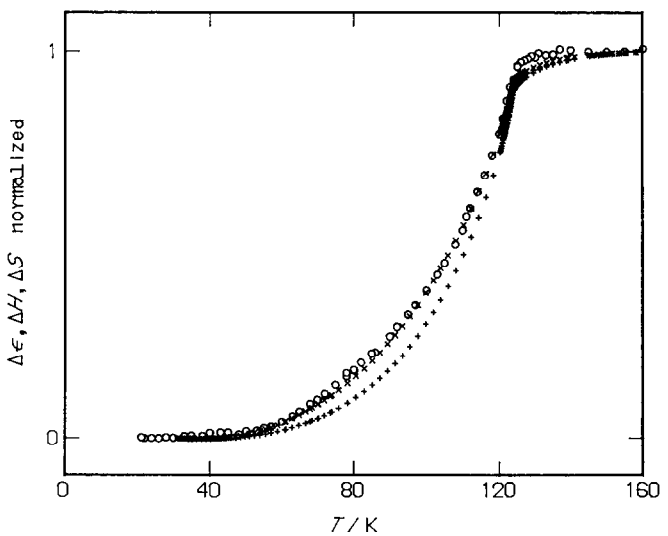

Fig. 10. Comparison of the dielectric permittivity (○), entropy (×), and enthalpy (+) of phase transition as a function of temperature in a normalized form.

revealed by neutron diffraction [5] results in the dielectric permittivity found here is not clear, relations between ϵ_{conf} and other experimental quantities are interesting. In Fig. 10, we plotted the excess enthalpy and entropy of transition as functions of temperature in a normalized form. The general features of the three curves are obviously very similar. They increase gradually at low temperatures and as the transition temperature is approached the slopes become infinite. Two further points are to be noted. First, the dielectric permittivity follows the entropy more closely than the enthalpy. The close correspondence between the entropy and permittivity may contain a clue to the interpretation of ϵ_{conf}. Second, the permittivity approaches the high temperature limiting value above T_c much faster than the enthalpy or entropy. For the latter two quantities, there are considerable contributions from the short-range order indicated by the excess heat capacity above T_c (see Fig. 2), whereas the short-range order effect is practically absent from the ϵ_{conf} vs. T curve. This suggests that ϵ_{conf} is proportional to the long-range order parameter. Further analysis in this direction would be fruitful but has not been pursued yet.

Finally, we point out that high frequency dielectric permittivity may provide information about the molecular mechanism of the phase transition and the dielectric response. The MA^+ ions reorient between two positions in the high temperature phase (at least in the analogous tin compound [5]) and the reorientation produces a dielectric response of $\Delta\epsilon = 0.08$. There will be a frequency between the radio and IR frequencies at which the reorientational motion causes dielectric absorption which our present measurement up to 100 kHz failed to detect.

CONCLUSION

We have shown that $(CH_3NH_3)_2[PtCl_6]$ undergoes a phase transition of higher order at 123.82 ± 0.05 K and have determined the transition enthalpy, transition entropy and critical exponents. The critical properties are close to those of the analogous tin compound. Thus the phase transition has a robust property: not only does it occur in a number of similar substances but its characteristics are also the same in different compounds, including the subtle details. Its dielectric property is unique among substances containing polar ions in that the permittivity follows the entropy in the temperature dependence, instead of obeying the Curie–Weiss law. It will be worthwhile to examine other substances showing similar phase changes using calorimetric as well as dielectric methods, preferably on single crystals.

REFERENCES

1 Y. Kume, R. Ikeda and D. Nakamura, J. Magn. Reson., 20 (1976) 276.
2 Y. Kume, R. Ikeda and D. Nakamura, J. Magn. Reson., 33 (1979) 331.

3 T. Matsuo, M. Ueda and H. Suga, Chem. Phys. Lett., 82 (1981) 577.
4 T. Matsuo, H.-K. Yan and H. Suga, J. Phys. Chem. Solids, 49 (1988) 85.
5 W.I.F. David, W.T.A. Harrison, R.C. Ward, A.J. Leadbetter, T. Matsuo and H. Suga, Physica, B156, 157 (1989) 96.
6 R. Ikeda, Y. Kume, D. Nakamura, Y. Furukawa and H. Kiriyama, J. Magn. Reson., 24 (1976) 9.
7 I.A. Oxton and O. Knop, J. Mol. Struct., 38 (1977) 25.
8 T. Matsuo and H. Suga, Thermochim. Acta, 88 (1985) 149.
T. Matsuo, Thermochim. Acta, 163 (1990) 57.
9 Y. Cho, M. Kobayashi and H. Tadokoro, J. Chem. Phys., 84 (1985) 4643.
10 R.W.G. Wyckoff, Am. J. Sci., 16 (1928) 349.
11 T. Sundius and M. Meinander, J. Mol. Struct., 76 (1981) 227.
12 M. Debeau and H. Poulet, Spectrochim. Acta, Part A, 25 (1969) 153.
13 T. Nakagawa and Y. Oyanagi, in K. Matsushita (Ed.), Recent Developments in Statistical Inference and Data Analysis, North Holland, The Netherlands, 1980.
14 H.E. Stanley, Introduction to Phase Transitions and Critical Phenomena, Clarendon Press, Oxford, 1971.
15 P. Schwartz, Phys. Rev. B, 4 (1971) 920.
16 W. Reese, Phys. Rev., 181 (1969) 905.
17 T. Matsuo and H. Suga, Solid State Commun., 21 (1977) 923.
18 M. Sekii, T. Matsuo and H. Suga, J. Incl. Phenom., 9 (1990) 243.
See also T. Matsuo, M. Sekii, H. Suga, N. Nakamura and H. Chihara, Z. Naturforsch., Teil A, 45 (1990) 519.
19 T. Matsuo, M. Tatsumi, H. Suga and S. Seki, Solid State Commun., 13 (1973) 1829.
20 M. Tatsumi, T. Matsuo, H. Suga and S. Seki, Bull. Chem. Soc. Jpn., 52 (1979) 716.
21 M. Oguni, T. Matsuo, H. Suga and S. Seki, Bull. Chem. Soc. Jpn., 48 (1975) 379.
22 J. Helwig, A. Klöpperpieper and H.E. Müser, Ferroelectrics, 18 (1978) 257.
23 M. Oguni, T. Matsuo, H. Suga and S. Seki, Bull. Chem. Soc. Jpn., 52 (1979) 941.
24 T. Matsuo, M. Månsson and S. Sunner, Acta Chem. Scand., Ser. A, 33 (1979) 781.
25 M. Fukai, T. Matsuo and H. Suga, J. Phys. Chem. Solids, 50 (1989) 743.
26 O. Yamamuro, T. Matsuo and H. Suga, J. Chem. Thermodyn., 18 (1986) 939.
27 H. Suga, Bull. Chem. Soc. Jpn., 34 (1961) 426.
28 A. Miyazaki, K. Sakata, M. Komukae, T. Osaka and Y. Makita, J. Phys. Soc. Jpn., 58 (1989) 3635.
29 A. Miyazaki, T. Ikeda, T. Osaka, M. Komukae and Y. Makita, J. Phys. Soc. Jpn., 58 (1989) 4496.
30 K. Kitahama, H. Kiriyama and Y. Baba, Bull. Chem. Soc. Jpn., 52 (1979) 324.
31 B. Szigeti, Proc. R. Soc. London, Ser. A, 261 (1960) 274.
32 E.B. Wilson, Jr., J. Chem. Phys., 3 (1935) 276; 6 (1938) 740.

APPENDIX A: CALCULATION OF THE ENERGY LEVELS OF INTERMOLECULAR AND INTRAMOLECULAR ROTATIONS OF MA^+ ION IN $(CH_3NH_3)_2[PtCl_6]$

The activation energies of the C_3 rotation of the MA^+ ion as a whole and of the internal reorientation of one end of the cation relative to the other have been determined from the NMR experiment [6] (the correlated and uncorrelated activation energies, as they are designated in ref. 6, are 3.6 kJ mol^{-1} and 8.5 kJ mol^{-1} respectively). The potential energies in which these motions take place can be described by the sinusoidal functions of appropriate angle variables. The amplitude of the sinusoidal potential may be

identified with the activation energy corrected for the zero-point vibration. The hamiltonian is given by

$$H = H_{fr} + V_u(1 - \cos 3\alpha)/2 + V_c(1 - \cos 3\chi)/2 \tag{A1}$$

Here α is the rotation angle of the $-CH_3$ group in the coordinate system fixed to the $-NH_3$ group, and χ is the rotation angle of the $-NH_3$ group relative to the coordinate system fixed to the crystal. H_{fr} is the hamiltonian of the free rotation of the two groups:

$$H_{fr} = \frac{\hbar^2}{2I_r}\left(\frac{d}{d\alpha} - \frac{I_r}{I_{NH}}\frac{d}{d\chi}\right)^2 - \frac{\hbar^2}{2I}\frac{d^2}{d\chi^2} \tag{A2}$$

$$I = I_{NH} + I_{CH} \tag{A3}$$

$$\frac{1}{I_r} = \frac{1}{I_{NH}} + \frac{1}{I_{CH}} \tag{A4}$$

Here, I_{NH} and I_{CH} are the moments of inertia of the NH_3 and CH_3 groups about the C_3 axis, respectively. The eigenvalues and eigenfunctions of the coupled-rotor hamiltonian were calculated by means of the expansion of the wavefunction in the eigenfunctions of H_{fr}, $|e^{in\alpha}> |e^{im\chi}>$, where $|n|$, $|m| \leqslant 10$ are the free rotational quantum numbers. This gave the lowest 441 levels. The character table of the group G' of the symmetry operations which leaves the hamiltonian unchanged is given in Table A1. There are 64 ($= 2^6$) spin functions [32]. They are decomposed as $16\Gamma_1 + 8\Gamma_2 + 8\Gamma_3 + 8\Gamma_4 + 8\Gamma_5 + 4\Gamma_6 + 4\Gamma_7 + \Gamma_8 + \Gamma_9$ according to G'. Symmetries of the basis $|e^{in\alpha}> |e^{im\chi}>$ are shown in Table A2. Allowed combinations of the spin and rotational functions are those for which the product representation contains the Γ_1 representation of the group G' when reduced to the irreducible

TABLE A1

The irreducible representation of group G' [a,b]

	E	C_3^C	$(C_3^C)^2$	C_3^N	$(C_3^N)^2$	C_3	C_3^2	$C_3^C C_3$	$C_3^N C_3$
Γ_1	1	1	1	1	1	1	1	1	1
Γ_2	1	1	1	ϵ^*	ϵ	ϵ^*	ϵ	ϵ^*	ϵ
Γ_3	1	1	1	ϵ	ϵ^*	ϵ	ϵ^*	ϵ	ϵ^*
Γ_4	1	ϵ^*	ϵ	1	1	ϵ^*	ϵ	ϵ	ϵ^*
Γ_5	1	ϵ	ϵ^*	1	1	ϵ	ϵ^*	ϵ^*	ϵ
Γ_6	1	ϵ^*	ϵ	ϵ^*	ϵ	ϵ	ϵ^*	1	1
Γ_7	1	ϵ	ϵ^*	ϵ	ϵ^*	ϵ^*	ϵ	1	1
Γ_8	1	ϵ^*	ϵ	ϵ	ϵ^*	1	1	ϵ^*	ϵ
Γ_9	1	ϵ	ϵ^*	ϵ^*	ϵ	1	1	ϵ	ϵ^*

[a] $\epsilon = \exp(2\pi i/3)$, $\epsilon^* = \exp(-2\pi i/3)$.

[b] In this table, C_3^C and C_3^N denote rotations of CH_3 and NH_3 respectively about the threefold axis through the angle $2\pi/3$ in a counter-clockwise direction. C_3 denotes the same rotation of MA^+ ion.

TABLE A2

Symmetries of basis ($|e^{in\alpha}> |e^{imx}>$) for the hamiltonian H [a]

m, n	$3k'$	$3k'+1$	$3k'-1$
$3k$	Γ_1	Γ_9	Γ_8
$3k+1$	Γ_3	Γ_5	Γ_6
$3k-1$	Γ_2	Γ_7	Γ_4

[a] In this table, k and k' are integers.

components. The spin function thus combined with each of the rotational states gives degeneracy of the energy level. In the actual calculation, it turned out that energy levels higher than those determined within the limited set of the basis functions contribute significantly to the heat capacity at higher temperatures. The size of the basis set has been limited by computer capacity. However, the distribution of the eigenvalues of the hindered rotators near the cut-off energy was similar to that of the free rotator eigenvalues. Therefore the eigenvalues of $H' = H_{\mathrm{fr}}$ + constant were used for $|n| > 11$ and $|m| > 11$, where the constant term is the difference between the spin-weighted means of the first 441 levels of the full and free rotator hamiltonians.

APPENDIX B: STANDARD THERMODYNAMIC FUNCTIONS

Standard thermodynamic functions were calculated by integration of the experimental heat capacity:

$$\Delta_0^T H^{\ominus} = \int_0^T C_p^{\ominus} \, \mathrm{d}T \tag{B1}$$

$$\Delta_0^T S^{\ominus} = \int_0^T \left(C_p^{\ominus}/T \right) \mathrm{d}T \tag{B2}$$

$$\Delta_0^T G^{\ominus} = \Delta_0^T H^{\ominus} - T \Delta_0^T S^{\ominus} \tag{B3}$$

In these equations, the superscript $^{\ominus}$ indicates the standard state to which the experimental condition was regarded as a good approximation. Table B1 gives the numerical values of the thermodynamic functions at rounded temperatures in the dimensionless form ($R = 8.3144$ J K^{-1} mol^{-1}).

TABLE B1

Standard chemical thermodynamic functions of methylammonium hexachloroplatinate in a dimensionless form

T (K)	$C^{\ominus}/R$	$\Delta_0^T H^{\ominus}/RT$	$\Delta_0^T S^{\ominus}/R$	$-\Delta_0^T G^{\ominus}/RT$
5	0.100	0.0199	0.0559	0.0359
10	0.658	0.1801	0.2699	0.0898
15	1.646	0.4934	0.7106	0.2172
20	2.957	0.9399	1.357	0.4174
25	4.473	1.493	2.177	0.6848
30	6.089	2.123	3.135	1.012
35	7.729	2.807	4.197	1.390
40	9.348	3.524	5.335	1.811
45	10.92	4.259	6.527	2.268
50	12.45	5.002	7.758	2.756
55	13.93	5.747	9.015	3.267
60	15.36	6.489	10.29	3.799
65	16.73	7.225	11.57	4.348
70	18.05	7.951	12.86	4.910
75	19.30	8.666	14.15	5.483
80	20.51	9.369	15.43	6.065
85	21.69	10.06	16.71	6.653
90	22.87	10.74	17.99	7.248
95	24.07	11.41	19.25	7.846
100	25.28	12.07	20.52	8.448
110	27.75	13.38	23.04	9.661
120	31.38	14.71	25.59	10.88
130	27.10	15.85	27.96	12.11
140	27.44	16.67	29.98	13.31
150	28.08	17.41	31.90	14.49
160	28.66	18.09	33.73	15.64
170	29.22	18.73	35.48	16.75
180	29.81	19.33	37.17	17.84
190	30.41	19.90	38.79	18.90
200	30.96	20.44	40.37	19.93
210	31.44	20.95	41.89	20.94
220	31.87	21.43	43.36	21.93
230	32.32	21.90	44.79	22.89
240	32.82	22.34	46.18	23.83
250	33.34	22.77	47.53	24.75
260	33.82	23.19	48.84	25.66
270	34.18	23.59	50.13	26.54
273.15	34.24	23.71	50.52	26.81
280	34.46	23.97	51.38	27.40
290	34.79	24.34	52.59	28.25
298.15	35.12	24.63	53.56	28.93
300	35.21	24.69	53.78	29.08